RSC Advances

PAPER

View Article Online
View Journal | View Issue

Cite this: *RSC Adv.*, 2026, **16**, 30017

Study of interfacial synergy in strontium-based organic framework/polyaniline/nanoporous graphene ternary composite as positive electrode for battery-supercapacitor hybrid devices

Gihan Abdelrahman Hassan Hammouda,[a] Ebraheem Abdu Musad Saleh,[a] Kashif Mahmud, *[b] Muhammad Zahir Iqbal,[c] Abhinav Kumar, [def] Asmaa Fathy Abd El-Aziz Kassem,[a] Nusiba Mohammed Modawe Alshik,[a] Ankit Dilipkumar Oza[gh] and Marwa Mostafa Moharam Haqqi Mohammed[a]

Received 3rd March 2026
Accepted 25th May 2026

DOI: 10.1039/d6ra01848c

rsc.li/rsc-advances

The escalating global demand for reliable and sustainable energy sources has intensified the need for advanced supercapacitor technologies capable of bridging the gap between capacitors and conventional batteries. However, the development of novel electrode material governing competitive specific capacity, energy and power density is critical. In this work, strontium-benzene tetracarboxylic acid metal–organic framework (Sr-BTCA) incorporated with PANI and NPG was synthesized and evaluated as an electrode material. Their synergistic integration of these components exploits their individual advantages. The electrochemical measurement demonstrates that Sr-BTCA/PANI/NPG based composite delivers specific capacity of 645.5 C g^{-1} at 1.5 A g^{-1}. Furthermore, the assembled two electrode hybrid device exhibit maximum energy density of 74.5 Wh kg^{-1}. Linear and quadratic models were applied on the experimental data to estimate the capacitive and diffusive contributions. The quadratic model provides a better fit on experimental as compared to the linear model which reveals that capacitive-controlled charge storage dominates at higher scan rates, confirming fast electrochemical kinetics. These results highlight the strong synergistic interaction among the MOF, PANI, and NPG components, positioning the Sr-BTCA/PANI/NPG composite as a promising electrode material for high-performance supercapacitor applications.

Introduction

The rapid evolution in the energy sector and the accelerating development in the use of portable electronics and electric vehicles has driven the demand for advanced energy technologies.[1] The conventional lithium batteries can achieve remarkable energy densities, yet challenges related to power density motivate for the exploration of alternate storage system such as supercapacitors. Supercapacitors are promising electrochemical energy storage devices owing to their rapid charge–discharge capability, high power density and excellent operational safety.[2,3] Sodium, lithium, and zinc-based systems offer high energy storage performance but share common limitations such as stability issues and limited cycling durability.[4,5] Although conventional supercapacitors offer many benefits, their lower energy density as compared to the rechargeable batteries prompt a major limitation, motivating intensive research into novel electrode materials capable of achieving superior energy storage performance without compromising power delivery.[6] Supercapacitors store energy through two principal mechanisms, fast and reversible faradaic redox processes, and electric double layer capacitance (EDLC), which arises from the electrostatic accumulation of charge at the electrode–electrolyte interface.[7,8] Advances in electrochemical systems, including biocathodes, electrocatalysts, and porous electrodes, highlight promising opportunities for efficient energy storage. Carbon based materials such as carbon nanotubes, activated carbon, and graphene derivatives are widely employed as composite-forming components in EDLC electrode materials due to their large surface area, chemical stability but their limited pseudocapacitive contribution often

[a]*Department of Chemistry, College of Science and Humanities in Al-Kharj, Prince Sattam Bin Abdulaziz University, Al-Kharj 11942, Saudi Arabia*
[b]*Riphah International University, Pakistan. E-mail: k.mahmud4051@gmail.com*
[c]*Unal Center of Education, Research and Development (UCERD), Rawalpindi, 44000, Pakistan*
[d]*Department of Technical Sciences, Western Caspian University, Baku, Azerbaijan*
[e]*Centre for Research Impact & Outcome, Chitkara University Institute of Engineering and Technology, Chitkara University, Rajpura, 140401, Punjab, India*
[f]*Department of Mechanical Engineering, Lloyd Institute of Engineering & Technology, Knowledge Park II, Greater Noida, Uttar Pradesh 201306, India*
[g]*Department of Mathematical Sciences, Saveetha School of Engineering, SIMATS, Chennai, 602105, Tamilnadu, India*
[h]*Department of Mechanical Engineering and Renewable Energy, Technical Engineering College, The Islamic University, Najaf, Iraq*

limit the achievable specific capacitance.[9–11] In contrast, the transition metal compounds and conductive polymers can offer higher capacitance, but they largely suffer from poor electron transport and structural instability during long operational cycles.[12,13]

Several composite based studies reflect the effects of MOF integration with PANI or NPG to significantly improve the performance of the supercapacitor electrode particularly in terms of specific capacity, energy and power density. Such as the enhanced performance exhibited by the PANI/NPG based supercapacitor returned a specific capacitance of 6.54 mF cm^{-2} with 9.11 mWh cm^{-2} and 1.56 W cm^{-2} energy and power density.[2] At 1 A g^{-1} current density, specific capacitance of 504 F g^{-1} was achieved by Co-MOF/PANI composite.[14] A carbon-based porous framework PC-MOFs/PANI delivered specific capacitance of 534.16 F g^{-1} at 0.2 A g^{-1}.[15] A sandwiched Zn-MOF/PANI composite resulting a specific capacitance of to 477 F g^{-1} at 1 A g^{-1}.[16] An Fe-MOF incorporated with PANI (Fe-MOF@PANI) demonstrated a specific capacitance of 234.6 F g^{-1} at 1 A g^{-1}.[17] A composite electrode material Sm-MOF/rGO/PANI displayed a significantly high specific capacitance of 1935.6 F g^{-1} with an energy and power density of 59.3 W kg^{-1} and 581 Wh kg^{-1} correspondingly.[18] The half-cell electrochemical performance of these materials was evaluated within medium potential window, as higher applied potentials may induce water splitting reactions, leading to electrolyte decomposition and reduced electrochemical stability.[19] Metal–organic frameworks have gained massive attention as an electrode material for supercapacitor due to their highly ordered porous structure, high specific surface area and chemically tunable composition.[20] By coordinating metal nodes with organic ligands provide abundant electroactive sites and adjustable pore structure which facilitate ion diffusion and adsorption.[21] Recently, a variety of MOFs, MOF derived materials and composites have been explored for energy storage exhibiting excellent performance. However, their intrinsically low electrochemical features of pristine MOFs restrict their electron transport leading to adverse effects on rate capability. The strontium-based metal–organic framework (Sr-BTCA), constructed using benzene tetracarboxylic acid (BTCA) as a coordinating ligand, is anticipated to offer exceptional structural stability along with readily accessible metal active sites, underscoring its promising potential as an electrode material for supercapacitor applications. The integration of strontium (Sr) metal centers is expected to enhance both the redox activity and the overall structural stability of the framework. Nevertheless, research into Sr-based MOFs for energy storage applications remains relatively scarce, and their electrochemical properties have yet to be comprehensively and systematically investigated.

Conducting polymers, particularly polyaniline (PANI), have emerged as highly attractive pseudocapacitive materials due to their exceptional capacitance, reversible redox behavior, low cost, and relatively straightforward synthesis procedures.[22] Although PANI benefit from multiple oxidation states that enable efficient faradaic charge storage, but their practical applications are limited by volumetric changes while rapid cyclic often cause mechanical degradation.[23] Hybridization of PANI with porous matrices is an effective approach to overcome these drawbacks while maintaining its pseudocapacitive performance. Porous, heteroatom-doped carbon materials and graphene-based materials show remarkable potential for energy storage applications.[24] Among these materials, nanoporous graphene (NPG) has gained particular attention owing to its well-interconnected pore structure, which is highly conducive to rapid ion diffusion, offers a high density of electrochemically active sites, and imparts enhanced mechanical and structural stability to the MOF framework.[25,26] In comparison with conventional 2-dimensional (2D) MXene and MOF composite offers superior electrochemical characteristics for electrode materials.[27] Material engineering strategies, particularly interfacial interaction and hybrid composite design, have been widely adopted to modulate the electrochemical properties. The rational integration of MOF, conductive polymer and graphene-based materials provide an effective approach to harness the complementary advantage of individual components. In such hybrid systems, MOF provide metal active sites and porosity, PANI contributes to enhanced pseudocapacitance and NPG promote rapid ion-transport and structural stabilization. Comprehensive investigations into ternary composites incorporating Sr-BTCA, PANI, and NPG remain considerably limited, and the underlying synergistic interactions that collectively dictate the electrochemical performance of such composites warrant further and more rigorous scientific investigation.

In this work, we report the synthesis and electrochemical evaluation of Sr-BTCA/PANI/NPG composite electrode material. The synergistic effects arising from the integration of these components were systematically investigated with respect to specific capacity, energy and power densities. Solvothermal method was followed for the synthesis of Sr-BTCA and Sr-BTCA/PANI/NPG composite. Structural, morphological and electrochemical characterizations were performed by employing SEM, XRD, EDX, CV, GCD and EIS. The Sr-BTCA/PANI/NPG delivered a specific capacity of 645.5 C g^{-1} at 1.5 A g^{-1}, while the two-electrode based hybrid device exhibited maximum energy and power density of 74.5 Wh kg^{-1} and 3200 W kg^{-1}. The capacitive and diffusive behaviour governed by the device was estimated through kinetic analysis by applying linear and quadratic models. This study provides valuable insight into the development of multifunctional hybrid electrode material and offers a viable strategy for developing high performance supercapacitors for energy storage.

Experimental

Materials

Strontium chloride dihydrate and 1,2,4,5-benzenetetracarboxylic acid were used as precursor materials. PVDF, NMP and acetylene black were utilized for the formation of slurry mixture. Ni foam was used as substrate. DI water and ethanol were used for washing steps.

Synthesis of Sr-BTCA

Strontium chloride dihydrate ($SrCl_2 \cdot 2H_2O$) was utilized as precursor material and dissolved in DI water. 1,2,4,5-

Benzenetetracarboxylic acid (H_4BTCA) was dissolved in *N*,*N*-dimethylformamide (DMF). Metal solution was slowly added to the ligand solution while continuously stirring for 20–30 min to achieve homogeneous mixtures. This mixture was further transferred to a sealed Teflon-lined autoclave for 16 hours at 160 °C. After cooling the solution, the product was obtained by subsequent centrifugation followed by washing, drying and finally material was obtained as powder form.

Synthesis of Sr-BTCA/PANI/NPG composite

A well-homogenized Sr-BTCA/PANI/NPG composite was obtained by physically mixing the Sr-BTCA, PANI and NPG in (2 : 1 : 1) ratio.

Preparation of working electrode

Nickle foam was cleaned thoroughly by ethanol, DI water and dilute HCl followed by drying in oven. A homogeneous slurry comprising 80% active material, 10% PVDF binder and 10% acetylene black in NMP was stirred for 6 hours and coated by drop casting on a 1 × 1 cm^2 nickel foam substrate and dried. The prepared electrode was subsequently subjected to electrochemical evaluation. The solvothermal preparation of Sr-BTCA and Sr-BTCA/PANI/NPG composite is depicted in Fig. 1.

Results and discussion

Morphological and structural analysis

X-ray diffraction (XRD) analysis was performed to determine the crystalline structure of the as prepared material of Sr-BTCA. The characteristic peaks exhibited by the diffraction pattern corresponds to the JCPDS #96-435-0449 indicating the formation of Sr-BTCA framework. The high intensity and sharpness of the peaks verify that the synthesized material exhibit good crystallinity and highly ordered porous network as shown in Fig. 2(a). For the Sr-BTCA/PANI/NPG, the diffraction pattern of Sr-BTCA were still present which indicate the preservation of the crystalline porous framework after the incorporation of PANI and NPG. The microstructural features and surface morphology of Sr-BTCA and Sr-BTCA/PANI/NPG composite were investigated through scanning electron microscopy (SEM) as shown in Fig. 2. SEM features for Sr-BTCA are represented in Fig. 2(b). It reveals a relatively uniform microcrystalline morphology comprised of rough surface and irregular shaped particles distributed homogeneously indicate successful nucleation and growth of porous framework by solvothermal process. The SEM image for Sr-BTCA/PANI/NPG reflects a relatively distinct morphology as portrayed in Fig. 2(c). A comparatively denser and more interconnected morphology is observed in the composite structure, which strongly indicates that PANI has effectively bridged with the Sr-BTCA framework, facilitating improved interfacial contact and structural integration between the two components, While NPG provide a conductive framework. Th presence of nanoporous graphene and polymeric coatings effectively reduces particle aggregation and enhance interparticle contact. Overall, SEM reflect that the structural integrity of the pristine does not disrupt by the integration of PANI and NPG but instead forms a more compact morphology which is favourable for supercapacitor electrodes to facilitate the transfer kinetics. The elemental composition and of the synthesized Sr-BTCA and Sr-BTCA/PANI/NPG were confirmed through energy-dispersive X-ray spectroscopy (EDX). The EDX spectrum of the pristine Sr-BTCA confirms the presence of Sr, C and O which reflect the successful formation of Sr-BTCA framework without detectable impurities as manifested in Fig. 2(d). The EDX spectrum for the

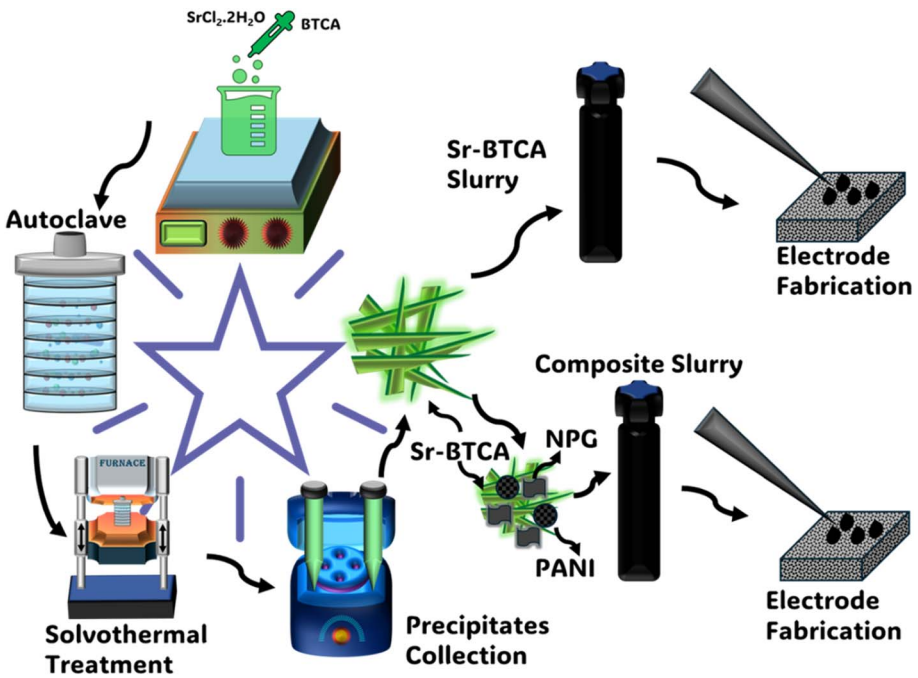

Fig. 1 Schematic illustration for the preparation of Sr-BTCA and Sr-BTCA/PANI/NPG composite.

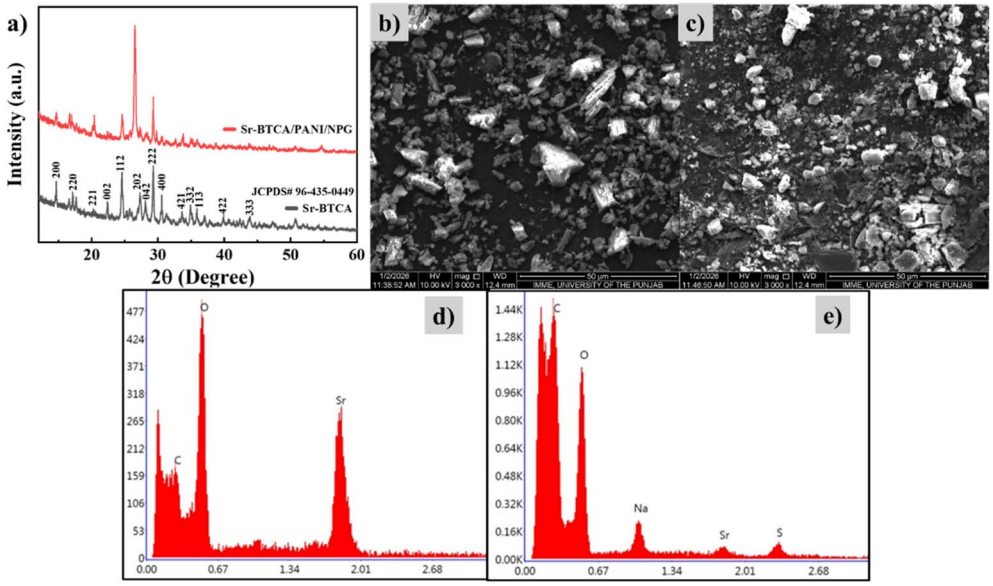

Fig. 2 (a) XRD patterns of Sr-BTCA and Sr-BTCA/PANI/NPG; SEM image of (b) Sr-BTCA (c) Sr-BTCA/PANI/NPG; EDX patterns for (d) Sr-BTCA (e) Sr-BTCA/PANI/NPG.

Sr-BTCA/PANI/NPG based composite corresponds to the contributions of porous species along carbonaceous components as demonstrated in Fig. 2(e).

Electrochemical analysis

Cyclic voltammetry (CV) was performed to access the electrochemical performance and charge storage mechanism of the prepared electrodes. Fig. 3(a) shows the CV behavior of the pristine Sr-BTCA electrode was investigated at various scan rates ranging from 3 to 50 mV s^{-1} within a potential window of 0.7 V. As the scan rates increases, the characteristic CV shape retained itself indicating good electrochemical stability within porous framework. Fig. 3(b) reflects the CV profile for Sr-BTCA/PANI/NPG composite recorded over the range of 3 mV s^{-1} to 50 V s^{-1}. Fig. 3(c) shows the comparative CV trend recorded at 3 mV s^{-1} for both Sr-BTCA and Sr-BTCA/PANI/NPG composite. The composite exhibit relatively larger integrated area and higher current response. Galvanostatic charge–discharge (GCD) profile of the electrodes was recorded to evaluate the capacitive performance. Fig. 4(a) and (b) displays the GCD curves of pristine Sr-BTCA and Sr-BTCA/PANI/NPG, respectively. The measurements were carried out at multiple current densities ranging from 1.5 A g^{-1} to 11 A g^{-1}, within a potential window of 0.6 V, to comprehensively evaluate the electrochemical performance of the electrode material. The discharge time decreases as the current density increases. In contrast, the composite exhibit significantly longer discharge time reflecting enhanced charge storage capability. A direct comparison between GCD curves recorded at 1.5 A g^{-1} for pristine and composite indicate the superior performance governed by the composite in terms of longer discharge times as portrayed in Fig. 4(c). The specific capacity of both electrodes was calculated through GCD data of multiple current densities as illustrated in Fig. 4(d). The Sr-BTCA/PANI/NPG exhibit higher specific capacity across the entire range of current densities as compared to the Sr-BTCA. These results highlight the effectiveness of formation of the composite by integrating Sr-BTCA with PANI and NPG to achieve enhanced electrochemical efficiency through synergistic

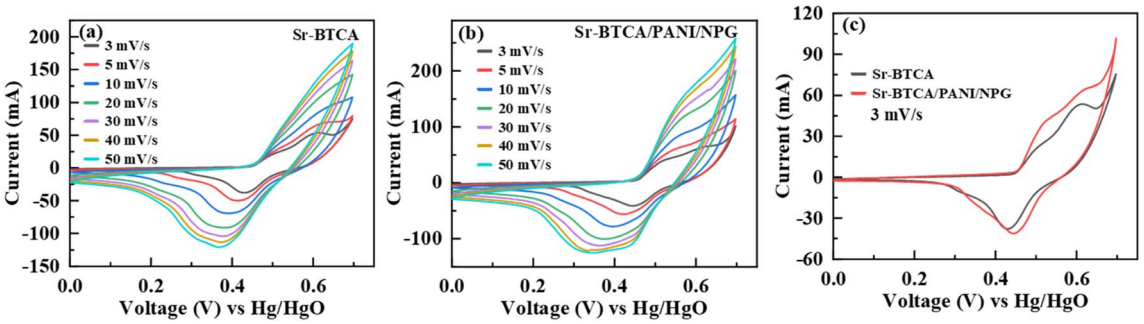

Fig. 3 Cyclic voltammetry trends at multiple scan rates for (a) Sr-BTCA (b) Sr-BTCA/PANI/NPG (c) Comparative CV trend at 3 mV s^{-1} for Sr-BTCA and Sr-BTCA/PANI/NPG.

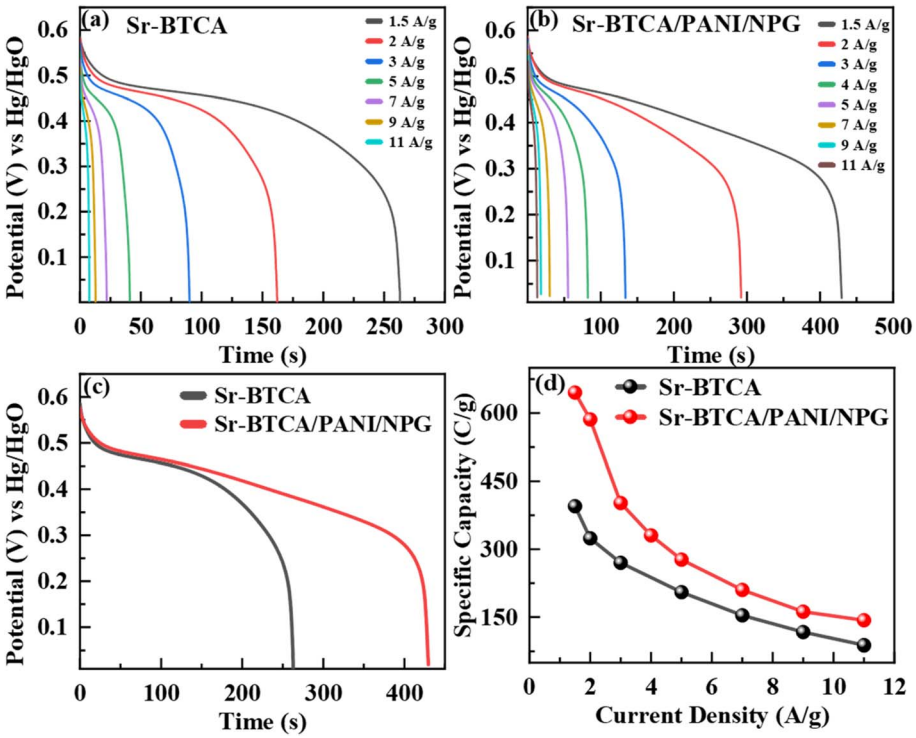

Fig. 4 GCD profiles at multiple current densities for (a) Sr-BTCA and (b) Sr-BTCA/PANI/NPG; (c) comparative GCD at 1.5 A g^{-1}, and (d) specific capacities at different A g^{-1}.

interaction between components. The following eqn (1) was employed to determine the specific capacity (Q_s).

$$Q_s = \frac{I \times \Delta t}{m} \quad (1)$$

where, I is the applied discharge current, Δt is the discharge time and m is mass of the active material. The specific capacity manifested by Sr-BTCA/PANI/NPG based composite and pristine Sr-BTCA was 645.5 C g^{-1} and 395 C g^{-1}, at 1.5 A g^{-1} respectively. Electrochemical impedance spectroscopy (EIS) was carried out to investigate the charge transfer resistance of the electrodes. Fig. 5(a) and (b) shows the real and imaginary components of the impedance for Sr-BTCA and Sr-BTCA/PANI/NPG respectively. The Nyquist plots of Sr-BTCA and Sr-BTCA/PANI/NPG are illustrated in Fig. 5(c). The high frequency regions correspond to charge transfer resistance (R_{ct}) while low frequency regions indicate Warburg impedance. The increased verticality of the composite and the reduced semicircular diameter confirmed improved ion-transport for the composite. The value of Equivalent Series Resistance (ESR) for Sr-BTCA and Sr-BTCA/PANI/NPG was determined to be 0.66 Ω and 0.46 Ω respectively.

Two-electrode assembly of the hybrid electrodes

A two-electrode cell was fabricated by employing Sr-BTCA/PANI/NPG composite material and activated carbon (AC) as the positive and negative electrode as displayed in Fig. 6(a). A comparative CV trend for battery grade Sr-BTCA/PANI/NPG and capacitive AC was obtained at 3 mV s^{-1} shooing their distinct characteristic curve shapes as represented in Fig. 6(b). A CV analysis of the Sr-BTCA/PANI/NPG//AC device was conducted within a potential window of 1.7 V across scan rates ranging from 3 to 100 mV s^{-1} as illustrated in Fig. 6(c). Similarly, a comprehensive galvanostatic charge–discharge (GCD) profiles of the Sr-BTCA/PANI/NPG//AC full device were recorded across

Table 1 Comparison of specific capacity/capacitance, energy density, and power density of the fabricated device with recently reported literature values

Hybrid device	Specific capacity or capacitance	Energy density (Wh kg^{-1})	Power density (W kg^{-1})	Cyclic stability	Ref.
CaCo-MOF@PANI@rGO//AC	192.8 C g^{-1}	78.7 Wh kg^{-1}	3086.9 W kg^{-1}	91.9%	28
MnLiS-MOF/PANI/rGO//AC	260 C g^{-1}	48 Wh kg^{-1}	1600 W kg^{-1}	91%	29
PM/CNT/MOF	650 F g^{-1}	45.93 Wh kg^{-1}	800 W kg^{-1}	72.7%	19
Sm-MOF/rGO/PANI//AC	218 F g^{-1}	59.3 Wh kg^{-1}	59.3 Wh kg^{-1}	91%	18
Sr-BTCA/PANI/NPG	645.5 C g^{-1}	74.5 Wh kg^{-1}	3200 W kg^{-1}	97.1%	This work

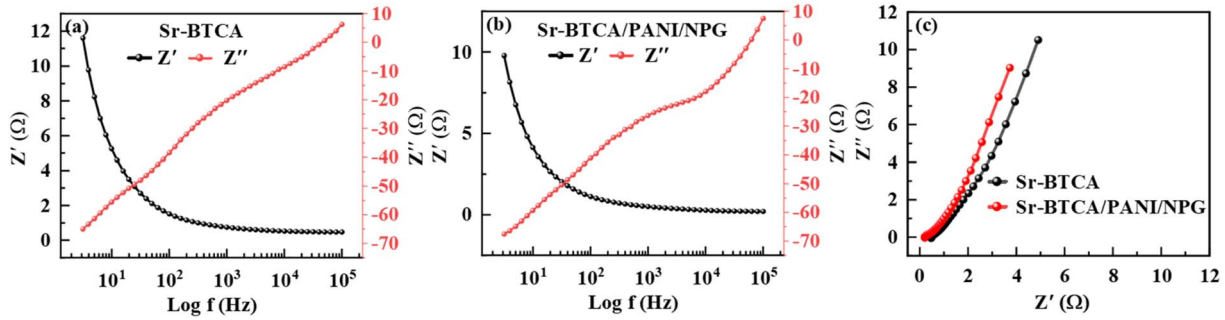

Fig. 5 Real and imaginary components of impedance as a function of frequency for (a) Sr-BTCA (b) Sr-BTCA/PANI/NPG (c) Nyquist plot.

multiple current densities ranging from 0.6 A g^{-1} to 5 A g^{-1}, within an operating potential window of 1.6 V, as illustrated in Fig. 6(d). The longer discharge time reveals the beneficial synergistic coordination of both electrodes. The specific capacity as a function of current density, derived from the GCD discharge time of the Sr-BTCA/PANI/NPG//AC device, is summarized in Fig. 7(a). The trends of specific capacity were found to be decreasing with increasing current density. The maximum specific capacity of 335.2 C g^{-1} was achieved at 0.6 A g^{-1}. Fig. 7(b) shows the Ragone plot for Sr-BTCA/PANI/NPG//AC to evaluate the relationship between the energy and power density providing insight into the electrochemical behaviour. The Sr-BTCA/PANI/NPG//AC deliver maximum energy and power density of 74.5 Wh kg^{-1} and 3200 W kg^{-1}, respectively. A comparative analysis of recently reported studies and the current study is summarized in Table 1. Following eqn (2) and (3) were followed to calculate the energy (E_S) and power density (P_S).

$$E_s = \frac{Q_s \times \Delta V}{2 \times 3.6} \quad (2)$$

$$P_s = \frac{E_s \times 3600}{\Delta t} \quad (3)$$

Here, ΔV attributes to potential window and Δt is the discharge time. Fig. 7(c) represent the Nyquist plot of the Sr-BTCA/PANI/NPG//AC hybrid device indicating low internal resistance and an overall capacitive behaviour. Fig. 7(d) demonstrates that the hybrid device retains 97.1% of its capacity after 5000 charge–discharge cycles.

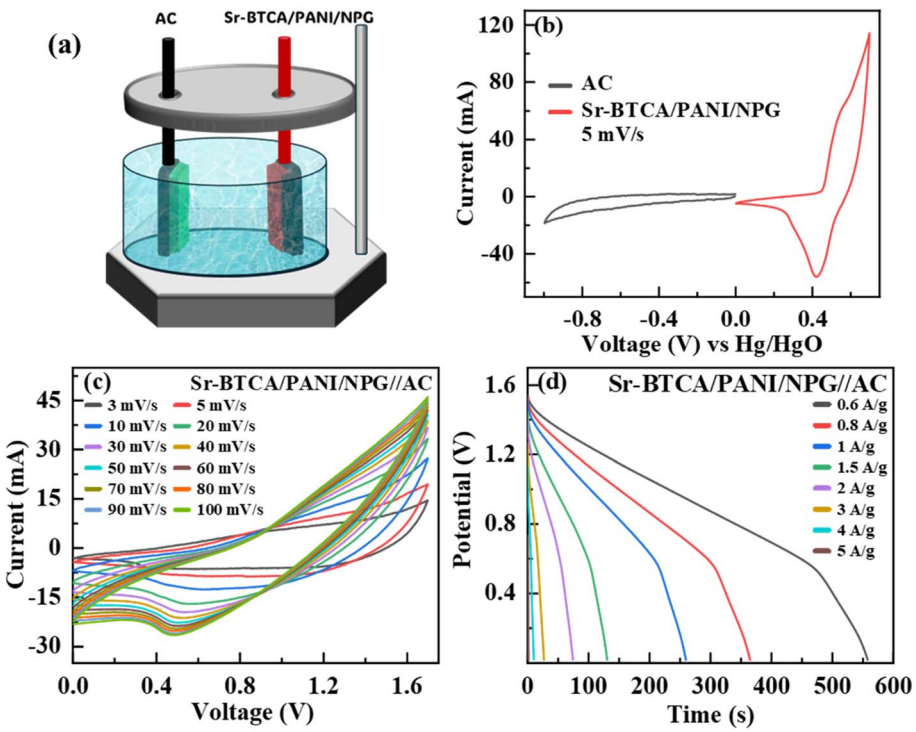

Fig. 6 (a) Sr-BTCA/PANI/NPG//AC hybrid device configuration, (b) comparative CV at 5 mV s^{-1}, (c) CV profile, and (d) GCD profile of the hybrid device.

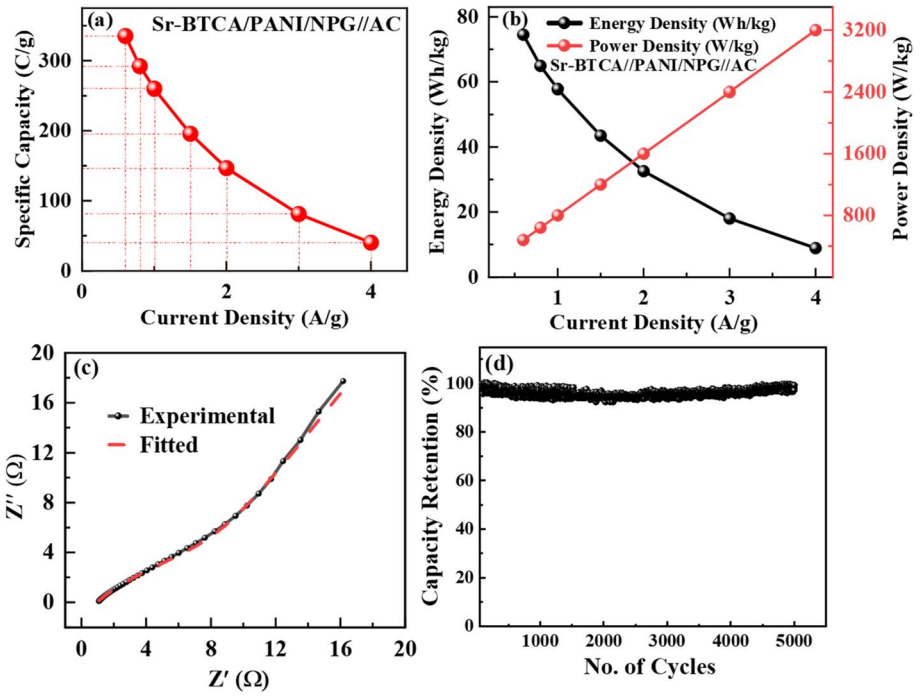

Fig. 7 Sr-BTCA/PANI/NPG//AC hybrid device, (a) specific capacity *vs.* current density, (b) Ragone plot, (c) impedance components, and (d) cyclic stability.

Estimation of the capacitive and diffusive contributions

Fig. 8(a), (b) and (c) display the analysis of capacitive and diffusive controlled contributions at 5 mV s^{-1}, 50 mV s^{-1} and 100 mV s^{-1} by using both linear and quadratic models. At lower scan rates, the diffusive controlled process dominates while at higher scan rates the capacitive behaviour was determined as

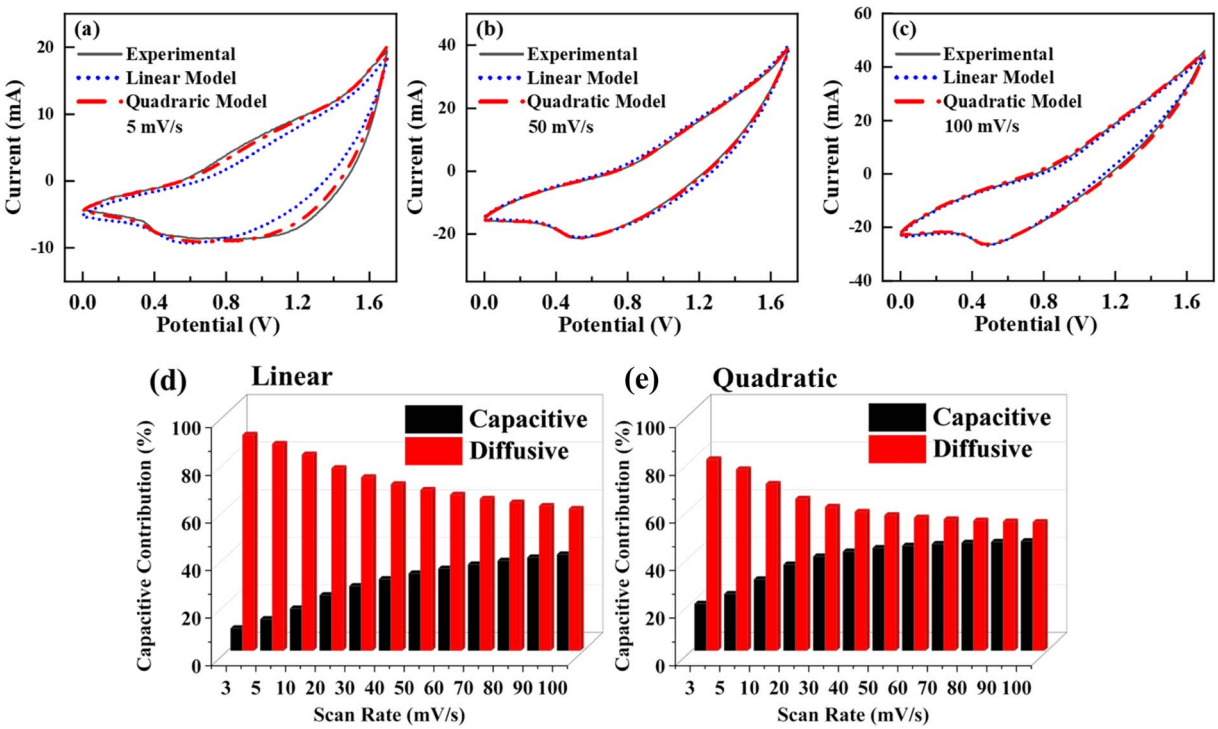

Fig. 8 Capacitive and diffusive contribution separation at (a) 5 mV s^{-1}, (b) 50 mV s^{-1}, and (c) 100 mV s^{-1}, percentage contributions estimated by (d) linear and (e) quadratic models.

dominant process which highlight effective surface utilization and rapid electrochemical kinetics of the hybrid electrode. Fig. 8(d) shows the percentage contribution of the capacitive and diffusive contributions attained through linear model across various scan rates. The diffusive contributions were decreasing with increasing scan rates while capacitive contributions were increasing progressively with increasing scan rates. At 5 mV s^{-1} the contributions were determined as highly diffusive. In contrast maximum capacitive behaviour was observed at 100 mV s^{-1}. The following eqn (4) was followed to quantify the linear model.

$$I(v) = k_1 v + k_2 v^{1/2} \quad (4)$$

In this, $k_1 v$ attributes to capacitive controlled contributions while $k_2 v^{1/2}$ refers to diffusive controlled contributions. Percentage capacitive and diffusive contributions were further attained through the quadratic model across various scan rates 3 mV s^{-1} to 100 mV s^{-1} as represented in Fig. 8(e). The eqn (5) was used for the estimation of quadratic model.

$$I(v) = k_1 v + k_2 v^{1/2} + k_3 v^{3/2} \quad (5)$$

Here, $k_1 v$ defines the combined effects of battery and supercapacitors (EDLC) while $k_2 v^{1/2}$ attributes to the battery type diffusion-controlled process and $k_3 v^{3/2}$ signifies the ohmic resistance. The percentage capacitive components contributions were found to be progressively improved with increasing scan rate. While the diffusion-controlled process diminished likewise. The highest diffusive process was exhibited at 5 mV s^{-1} while maximum capacitive behaviour was obtained at 100 mV s^{-1} scan rate which confirms effective surface utilization of the hybrid electrode. Overall, the comparison of the two approaches reveals that quadratic model more accurately fit the experimental data than the linear model demonstrating its capability to capture the capacitive and diffusive controlled processes in a better way.

Conclusion

In summary, Sr-BTCA/PANI/NPG based novel ternary composite was prepared to address the intrinsic limitations of the individual components for supercapacitor applications. The porous framework of Sr-BTCA provides abundant electrochemically active sites, incorporation of PANI improve pseudocapacitive charge storage while NPG serves as an efficient conductive scaffold to improve ion-transport. As a result of the synergistic cooperation, the composite electrode exhibits a specific capacity of 645.5 C g^{-1} while the pristine Sr-BTCA delivers 395 C g^{-1}. A hybrid two-electrode device Sr-BTCA/PANI/NPG//AC demonstrating a competitive energy density of 74.5 Wh kg^{-1} and its maximum power density of 3200 W kg^{-1} reflecting its practical applicability. Comprehensive analysis by employing the semi-empirical models reveals that capacitive contributions dominate at higher scan rates confirming efficient electrode utilization and rapid charge transfer. Overall, this study demonstrates strong potential of Sr-BTCA/PANI/NPG composite-based hybrid electrode for next generation high performance supercapacitor devices.

Author contributions

Gihan Abdelrahman Hassan Hammouda: project administration, conceptualization, funding acquisition. Ebraheem Abdu Musad Saleh: writing – review & editing, formal analysis. Kashif Mahmud: writing – original draft, data curation, methodology, formal analysis. Muhammad Zahir Iqbal: project administration, writing – review & editing, investigation, software, formal analysis, conceptualization. Abhinav Kumar: formal analysis. Asmaa Fathy Abd El-Aziz Kassem: writing – review & editing, formal analysis. Nusiba Mohammed Modawe Alshik: writing – review & editing, formal analysis. Ankit Dilipkumar Oza: writing – review & editing. Marwa Mostafa Moharam Haqqi Mohammed: writing – review & editing, formal analysis.

Conflicts of interest

There are no conflicts to declare.

Data availability

This article contains no supplementary data. All data relevant to this study are included within the manuscript.

Acknowledgements

The authors extend their appreciation to Prince Sattam bin Abdulaziz University for funding this research work through the project number (PSAU/2025/01/34415).

References

1 S. Chu and A. Majumdar, Opportunities and challenges for a sustainable energy future, *nature*, 2012, **488**(7411), 294–303.
2 K.-U. Lee, *et al.*, A high-performance supercapacitor based on polyaniline-nanoporous gold, *J. Alloys Compd.*, 2019, **779**, 74–80.
3 X. Li, *et al.*, Hydroxyl-Rich Hyperbranched Polyglycerol Additive for Low-Temperature Aqueous Zinc Batteries: Sustained and Efficient Dehydration and High-Conductivity, *Advanced Science*, 2026, **13**(7), e16639.
4 L. Xu, *Electrode Materials in Energy Storage Technologies: Applications in Lithium-, Sodium-, Potassium-, Sulfur-And Zinc-Based Rechargeable Batteries*, John Wiley & Sons, 2025.
5 T. Long and Y. Guo, Research on the temperature radius stratification model based on electrochemical-thermal-force coupling in Lithium-ion batteries, *Electrochem. Commun.*, 2025, 108052.
6 K. S. Lakshmi and B. Vedhanarayanan, High-performance supercapacitors: a comprehensive review on paradigm shift of conventional energy storage devices, *Batteries*, 2023, **9**(4), 202.

7 Y. Shao, *et al.*, Design and mechanisms of asymmetric supercapacitors, *Chem. Rev.*, 2018, **118**(18), 9233–9280.
8 A. A. Almunyif, S. Mumtaz and A. M. Afzal, Synergistic Ni (OH) $_2$@ $Li_4Ti_5O_{12}$@ B/N-doped graphene architecture: Pioneering high-energy hybrid supercapacitors with superior electrocatalytic performance, *Inorg. Chem. Commun.*, 2025, 115243.
9 S. K. Kandasamy and K. Kandasamy, Recent advances in electrochemical performances of graphene composite (graphene-polyaniline/polypyrrole/activated carbon/carbon nanotube) electrode materials for supercapacitor: a review, *J. Inorg. Organomet. Polym. Mater.*, 2018, **28**(3), 559–584.
10 P. Sinha, S. Banerjee, and K. K. Kar, Activated carbon as electrode materials for supercapacitors, in *Handbook of Nanocomposite Supercapacitor Materials II: Performance*, Springer, 2020, p. 113–144.
11 S. Mumtaz, *et al.*, Enhanced charge carrier transit in NiMoO4-CNTs nanocomposites grown on carbon paper for flexible hybrid supercapacitors and electrochemical cholesterol sensing, *Inorg. Chem. Commun.*, 2025, 115255.
12 B. De, *et al.*, Transition metal oxides as electrode materials for supercapacitors, in *Handbook of Nanocomposite Supercapacitor Materials II: Performance*, Springer, 2020, p. 89–111.
13 W. Qin, *et al.*, Activated carbon coated with polyaniline as an electrode material in supercapacitors, *N. Carbon Mater.*, 2008, **23**(3), 275–280.
14 R. Srinivasan, *et al.*, Enhanced electrochemical behaviour of Co-MOF/PANI composite electrode for supercapacitors, *Inorg. Chim. Acta.*, 2020, **502**, 119393.
15 M. Yao, *et al.*, Polyaniline nanowires aligned on MOFs-derived nanoporous carbon as high-performance electrodes for supercapacitor, *Electrochim. Acta*, 2021, **390**, 138804.
16 S. Guo, *et al.*, (Metal-Organic Framework)-Polyaniline sandwich structure composites as novel hybrid electrode materials for high-performance supercapacitor, *J. Power Sources*, 2016, **316**, 176–182.
17 M. Kumar, *et al.*, PANI Incorporated Fe-MOF: As an Electrode Material for Supercapacitor, *J. Ravishankar Univ. (Part-B)*, 2024, **37**(2), 195–205.
18 S. Rajasekaran, *et al.*, Sm-MOF/rGO/PANI composite as an electrode material for supercapacitor applications, *Electrochim. Acta*, 2023, **467**, 143031.
19 G. Wang, H. Wang and J. Bai, Preparation and electrochemical evaluation of manganese ferrite spheres as anode materials for half and full lithium-ion batteries, *J. Alloys Compd.*, 2015, **627**, 174–181.
20 S. Kitagawa, Metal–organic frameworks (MOFs), *Chem. Soc. Rev.*, 2014, **43**(16), 5415–5418.
21 Y. Peng, *et al.*, Metal–organic frameworks as electrocatalysts, *Angew. Chem., Int. Ed.*, 2023, **62**(9), e202214707.
22 H. Wang, J. Lin and Z. X. Shen, Polyaniline (PANi) based electrode materials for energy storage and conversion, *J. Sci. Adv. Mater. Devices*, 2016, **1**(3), 225–255.
23 H. R. Zhang, H. L. Li and J. X. Wang, Capacitance fading induced by degradation of polyaniline: cyclic voltammetry and SEM study, *Adv. Mater. Res.*, 2012, **535**, 1205–1209.
24 J. Liu, *et al.*, Graphene-based materials for energy applications, *MRS Bull.*, 2012, **37**(12), 1265–1272.
25 F. Yang, *et al.*, Polydopamine chelating strontium on graphene oxide enhances the mechanical and osteogenic induction properties of PLLA/PGA bone scaffold, *Int. J. Bioprint.*, 2024, **10**(3), 1829.
26 H. Huang, *et al.*, The chemistry and promising applications of graphene and porous graphene materials, *Adv. Funct. Mater.*, 2020, **30**(41), 1909035.
27 M. Jalalah, *et al.*, Green synthesis of Bi-metallic MXene (Mo2TiC2Tx)@ NiCo-MOF@ AC nanocomposite electrode for high-performance electrochemical energy storage, HER, ORR and photochemical applications, *Ceram. Int.*, 2025, **51**, 47417–47431.
28 H. Osman, *et al.*, Development of CaCo-MOF@ PANI@ rGO hybrid electrodes for enhanced energy storage and hydrogen evolution reaction performance, *Mater. Chem. Phys.*, 2025, 131689.
29 M. S. Khan, *et al.*, Synergistic Electrochemical Performance of Mn-Li-S MOF Integrated with PANI/rGO for Supercapattery and Hydrogen Production Applications, *Micro Nanostruct.*, 2025, 208367.